RSC Advances

ROYAL SOCIETY OF CHEMISTRY

www.rsc.org/advances

Cite this: DOI: 10.1039/c0xx00000x

www.rsc.org/xxxxxx

ARTICLE TYPE

Nitrogen-doped graphene as a cathode material for dye-sensitized solar cells: effects of hydrothermal reaction and annealing on electrocatalytic performance

Yake Zhang, Zhe Sun, * Wang Hui, Yudan Wang, Mao Liang and Song Xue*

Received (in XXX, XXX) Xth XXXXXXXXX 20XX, Accepted Xth XXXXXXXXX 20XX
DOI: 10.1039/b000000x

We prepared nitrogen doped graphene (NG) by reacting pristine graphene oxide (GO) with urea hydrothermally and elucidated its usage as Pt-free cathode material in the DSCs based on cobalt based redox shuttles. In the process of hydrothermal reaction, the graphene oxide sheets are kept in a flocculating state. This experimental protocol prevents the graphene sheets from gelation and yields a maximum nitrogen content of 7.6 at%. The resultant NG sediments can be readily deposited onto conductive glass sheet for fabricating porous cathode. The content ratio of the doped nitrogen atoms to the residual oxygen atoms is demonstrated as a determinant factor affecting the electrocatalytic activities of the as-prepared NG sheets. Annealing treatment to the NG cathodes gives rise to a remarkable increase of exchange current density. Moreover, the XPS results indicate that the electrochemically active pyridinic-N groups formed in the early stage of hydrothermal reaction are unstable to annealing. However, their thermal stability can be improved by extending the time of hydrothermal reaction. By optimizing the composition of the embedded nitrogen species and oxygen containing groups, the DSCs with NG cathode yield a maximal device efficiency of 8.2 %.

1. Introduction

Dye-sensitized solar cell (DSC) has drawn widespread attentions as a promising candidate to replace silicon-based solar cell owing to its low cost in device fabrication, easy tunable optical response, and relative higher power conversion efficiency.[1-4] A typical DSC assembly consists of a sensitizer anchored titania film for harvesting incident light and collecting photo-generated electrons, a platinized counter electrode for loading the separated positive charges, and an iodine based electrolyte solution for recovering sensitizer cations. Although iodide/triiodide functions well in charge separation, this redox couple exhibits large loss-in-potential during dye regeneration, undesirable absorption of the blue part of sunlight spectrum, and corrosion to Ag or Cu current collectors.[5,6] For these reasons, a variety of iodine-free redox mediators, especially cobalt complex based redox shuttles, have been explored extensively. [7-9] Several pioneering works have reported power conversion efficiency (PCE) for the DSCs with cobalt complex $[Co(bpy)_3]^{2+/3+}$ in combination with Zn-porphyrin sensitizers exceeding 12 % under the irradiation of 100 mW cm^{-2}. [10-12] Yum et al. addressed that the employment of hole-conducting polymer (PProDOT) cathode in place of Pt counter electrode can improve the photovoltaic performance of the DSCs based on tridendate cobalt complex $[Co(bpy\text{-}pz)_2]^{3+/2+}$ because the former exhibits a 20-fold decrease of charge transfer resistance (R_{ct}) at electrolyte/cathode interfaces.[13] Similar observations have also been reported for the DSCs with thiolate/disulfide or copper complex redox shuttle.[14-18] Nanoporous electrodes based upon CoS,[19,20] MoS_2,[21] PEDOT,[15,22] and carbon black,[14] show the electrochemical activity comparable to or even better than platinized counter electrode, and give rise to a higher fill factor (FF). With this regard, the replacement of platinum catalyst by the alternative materials not only plays a role in reducing the production cost and improving long-term stability in corrosive electrolyte, but also leading to an outperforming electrocatalytic activity in the regeneration of redox mediators.

Graphene has emerged as an intriguing nanomaterial because of its large surface area, fast carrier mobility, and tunable sheet size. Up to now, this material has been explored for various applications, including energy storage, field effect transistors, sensors, and so forth.[23,24] When serving as a cathode material for DSCs, heteroatom doped graphene instead of bare graphene is more effective because the embedding of nitrogen, boron, sulfur, or oxygen atoms into graphene carbon lattice gives birth to more electrochemical active sites and tailors the band gap of graphene simultaneously.[25-30] Recently, reduced graphene oxide (RGO) and commercialized graphene sheets embedded with oxygen-containing groups were employed as the electrochemical catalyst alternative to platinum. [31-34] These works showed that the ratio of oxygen to carbon in graphene architecture is highly relative to the catalytic activity. However, the increase of the ratio of oxygen to carbon is constrained by the conductivity of graphene sheets, implying a balance between redox reaction and charge transport.

The employment of nitrogen doped graphene (NG) as DSC cathode gives a potential solution to the contradiction between catalytic activity and conductivity.[35,36] Lone pair electrons of the embedded nitrogen atoms render additional electrochemical activity to graphene skeleton. Meanwhile, nitrogen-containing functional groups, such as pyridinic, pyrrolic, quaternary and N-oxide of pyridinic N, are highly conjugated to the π system, which engenders a lower internal resistance to the transport of positive charges inside graphene sheets.[37] One of the obstacles hinders the persisting improvement of nitrogen doped graphene nanosheets as cathode material is their poor adhesion to FTO substrates. The resultant series resistances at NG/FTO interfaces deteriorate the charge transfer from NG sheets to FTO layers remarkably. To ameliorate the interfacial contact, graphene oxide (GO) was employed as binder in the fabrication of mechanically stable cathode.[31,37] An alternative route to improve the adhesion strength is the embedding of oxygen containing moieties and nitrogen groups into graphene framework, simultaneously.[38] For realizing this attempt, hydrothermal reaction with GO and urea can be employed. In this scenario, nitrogen doping process is accompanied by the reduction of oxygen groups. Sun et al. and other groups have demonstrated that a part of oxygen groups is preserved at graphene skeleton after hydrothermal process.[39,40] Apart from maintaining the needed adhesiveness, the hydrothermal reaction pathway also exhibit the advantages of low-cost and facile. However, several works have shown that the resultant NG rends to form a 3D cross-linking structure due to the cyclization or esterification reactions bewteen the adjoining graphene frameworks.[39,41] Since the gelation structure has an invariable geometry, it is unsuitable to fabricate homogeneous NG layer with the thickness at micrometer scale.

In this work, we prepared NG nanosheets via a hydrothermal procedure by using urea as a cheap and abundant nitrogen source. A different strategy employed here is that GO is maintained in a flocculent state during hydrothermal preparation. In this way, the gelation of GO during the hydrothermal process is avoided, which facilitates the deposition of homogenous NG layer onto FTO sheets. Unlike planar platinized cathodes,[31] the NG cathodes in this work are featured as nanoporosity. As illuminated by Papageorgiou et al.,[42,43] such structure decreases the redox reaction overpotential of the cathodes considerably and hence extends the useful current scope during the operation of DSCs. Therefore, the NG cathode with a porous structure deserves an extensive exploration although many studies have focused on planar graphene based cathodes. Here we evaluated the electrocatalytic activities of nanoporous NG cathode in the reaction of cobalt complex redox couples by using electrochemical impedance techniques (EIS). It was shown that the N/O atomic ratio determined by hydrothermal reaction time is critical to the electrocatalytic performance. Also the effects of the annealing treatment to the NG cathodes were further elucidated. With the optimized NG cathode, the DSCs based on organic dye XS57 (chemical formula in the ESI†) in combination with $Co(phen)_3^{2+/3+}$ redox couple yield the PCE of 8.6 %, exceeding the performance of the DSCs with Pt cathode.

2. Experimental section

2.1 Materials and Preparation of Counter Electrodes

Graphene oxide (GO) was synthesized from natural graphite flakes (100 mesh, Aldrich) by a modified Hummer's method.[45] The as-prepared GO was employed in the preparation of nitrogen doped graphene (NG) via a hydrothermal process. In a typical experiment, 60 mg of GO was dispersed into 60 ml of deionized water by vigorous stirring (ca. 20 min). The resultant homogeneous suspension was mixed with 3.5 mL of concentrated H_2SO_4 (98%), which gives rise to immediate flocculation of dark-brown GO sheets from the solution. After that, this mixture was added with 3.6 g of urea as a nitrogen source, and stirred for 15 min. The urea-containing dispersion was then transferred into a 100 mL Teflon-lined autoclave and heated at 180 ^oC for 2~18 hrs. The resultant coagulative precipitate was filtered and washed with a mixing solution of ethanol/water (v/v 1:1) for several times until pH value of 7.0 is attained. Afterwards, the filtrate was concentrated by centrifugation at 3500 rpm for 30 min, giving the final paste containing 85 wt % of NG nanosheets.

Cathode based on nitrogen doped graphene was fabricated by depositing the as-prepared NG paste onto a FTO glass sheet (Nippon Sheet Glass, 15 Ω/square) by using a doctor blade technique. A 60 μm tape (Scotch, USA) was employed as a spacer for controlling the thickness of graphene layer at ~ 17 μm. Before assembled with a dye soaked TiO_2 electrode, wet counter electrode was dried at 80 ^oC for 15 min, or further annealed at 350 ^oC for 2 hrs. NG-2, NG-6, NG-12, and NG-18 mark the dried cathodes based on the NG sheets prepared hydrothermally for 2, 6, 12, and 18 hrs, respectively. And NG-2S, NG-6S, NG-12S, and NG-18S represent the annealed NG cathodes correspondingly. The loading amount of NG in the cathodes dried at 80 ^oC is 1.70 mg cm^{-2}. By contrast, the loading amount of the NG cathodes annealed at 350 ^oC is about 1.19±0.06 mg cm^{-2}. The error arises from the difference of the elemental composition of the NG samples, which leads to the variation of weight loss under heat treatment. In addition, platinized cathode was prepared by spin-coating H_2PtCl_6 solution (50 mM, in 2-propanol) onto the FTO glass and calcining at 395 ^oC for 15 min. The loading amount of Pt on the substrate is 17.2 μg cm^{-2}.

2.2 Cell Fabrication

Nanoporous photocathode was prepared by screen-printing a colloidal paste containing 20 nm sized TiO_2 particles onto a FTO glass pretreated by aqueous $TiCl_4$ solution. Detailed procedures of TiO_2 paste fabrication and the treatment of FTO glass sheet have been described previously.[46] The TiO_2 coated electrode with an active area of 0.158 cm^2 was calcined at 500 °C in air for 30 min, giving the resultant thickness of ~ 5 μm. After cooled to 80 °C, the TiO_2 electrode was sensitized by immersing it into a 0.3 mM organic dye (3-[6-[4-[4'-dihexyloxybiphenyl-4-yl-amino-] phenyl [-4,4'-dihexylcyclopenta-[2,1-b:3,4-b]dithiphene-2-yl]-2-cyanoacrylic acid, coded XS57) solution with a mixed solvent of dichloromethane/ethanol (v/v: 1:4) at room temperature.[47] After soaked for 24 h, the sensitized TiO_2 film was rinsed with anhydrous ethanol and dried by air flow. The cathode possessing an electrolyte-filling hole of 1 mm diameter was then assembled with the TiO_2 film. A 25 μm thick Surlyn hot-melt gasket (Solaronix, Switzerland) was employed for sealing and separating the electrodes. The leaved space in the sandwich DSC was filled with cobalt based electrolyte containing 0.25 M $[Co(II)(phen)_3](PF_6)_2$, 0.05 M $[Co(III)(phen)_3](PF_6)_3$, 0.5 M 4–

tertpyridine (TBP) and 0.1M LiTFSI in acetonitrile.

The assembly of symmetrical dummy cell was conducted by using two identical cathodes. One of them has a hole for perfusing electrolyte solution. For electrochemical testing, the circle graphene film loading on the FTO glass sheet has the active of 0.196 cm^2. The dummy cell was thermally sealed with Surlyn hot-melt gasket before filling with the cobalt electrolyte used in the fabrication of DSC. Actual distance between the graphene films is around 60 μm as determined by a digital micrometer.

2.3 Characterization Techniques

The morphology of nitrogen doped graphene was obtained by using JEM-2000 transmission electron microscopy (TEM, JEOL). A diluted NG/ethanol dispersion after vigorous sonication was dropped onto a Cu micro-grid for TEM recording. SEM characterization was carried out with a Nova Nano SEM 230 (FEI, USA). WAXS measurements were performed by a D/max-2500 X-ray diffractometer (Rigaku, Japan) with Cu-K a radiation at a scanning speed of 1° /min. FT-IR spectra were collected by a Tensor 27 FT-IR spectrometer (Bruker, Germany) using the transmission mode at the resolution of 4 cm^{-1}. XPS analysis on nitrogen doped graphene was performed on a K-alpha X-ray photo-electron spectrometer (ThermoFisher, USA) with an Al-Kα (1486.6 eV) achromatic X-ray source. Current-voltage (J–V) characteristics were recorded by a computer controlled Keithley-2400 digital source meter (Keithley, USA). A standard solar simulator equipped with a 300 W xenon lamp and an AM 1.5 filter (Oriel 91160-1000, Newport, USA) was employed as the irradiation source. Illumination intensity was adjusted to 1 sun (100 mW cm^{-2}) by using a NREL-calibrated Si solar cell. Electrochemical impedance spectra (EIS) of the symmetrical dummy cells were determined by a Zennium electrochemical workstation (ZAHNER, Germany). The EIS measurements are also performed for characterizing the DSCs at bias voltage of 0.8 V in the dark. Scanning frequency ranges from 200 kHz to 0.2 Hz, and the modulation amplitude was fixed at 10 mV.

3. Results and Discussion

The hydrothermal preparation of NG nanosheets was carried out by using the precursor of acidic GO/urea dispersion. In this precursor, GO was flocculated from the solution due to the excessive protons. (Fig. S1†). We found that this pretreatment successfully prevents the gelation of GO during hydrothermal reaction. The resultant NG products after drying at 80 °C are pulverous and contain the embedding nitrogen atoms of ~ 7 at% according to XPS measurements (see below for detail). This result indicates that the flocculation does not affect the reaction activity of GO in the process of nitrogen doping. In practice, the morphology of GO floccules in the dispersion is loose and fractal, which brings out sufficient contact surfaces for embedding nitrogen atoms into graphene lattice. At the same time, the flocculation also reduces the possibility of the collision of GO nanoplatelets, by which gelation reaction is quite limited.

The morphologies of NG nanosheets dried at 80 °C are displayed in Figure 1a and b. These images indicate that NG based cathode (shown in the inset of Fig. 1a) exhibits a highly wrinkled conformation in the scale of nanometer. Such disorder structure implies a less sufficient interlayer π-π stacking, originating from the doping of nitrogen atoms and the incomplete reduction of oxygen containing groups in the hydrothermal reaction. Apparently, the wrinkles enhance the area of NG surface available to the regeneration of cobalt redox couple. And it was also reported that the crumpled conformations are associated with the mid-gap states which give rise to the enhancement of catalysis activity due to the additional chemisorption abilities.[48,49] We further found that the amorphous NG film can be readily exfoliated into the nanosheets by using ultrasonic dispersion. In Fig. 1c, transparent nanosheets of NG are observed, which shows a lamellar stacking structure with several foldings. Obviously, gelling clusters are invisible implying the validity of our procedure in limiting the gelation. Moreover, the crystallization behaviours of NG and pristine GO are shown in Fig. 1d with the aid of XRD patterns. It is observed that the pristine GO exhibits a sharp diffraction peak at 11.2 °, corresponding to a layer by layer structure with d_{002} of ~0.79 nm as reported previously.[50,51] By contrast, XRD peak of NG shows a board shape centering at ~ 25.1°, namely an interlayer space of ~0.34 nm. The degree of order is close to the undoped graphene with a strong peak at 25.8 °, reflecting a self-healing of graphitic crystal structure concomitant to nitrogen embedding.[52]

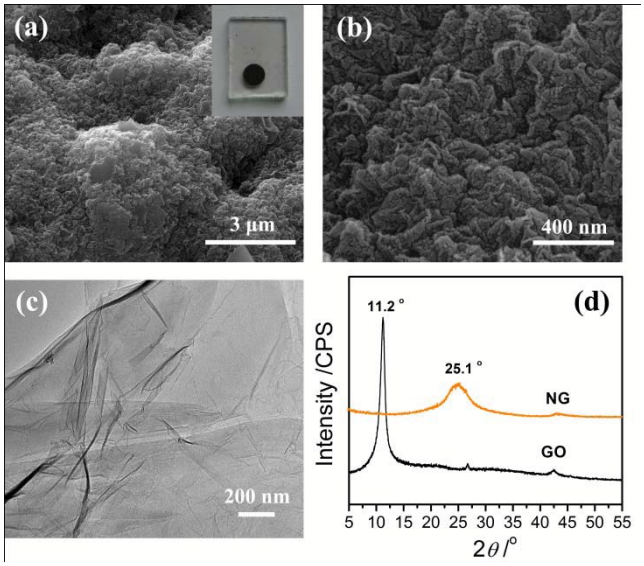

Fig. 1 SEM images (a and b) and TEM image (c) of nitrogen doped graphene (NG); (d) XRD patterns of NG and pristine graphene oxide (GO). Inset of (a) shows the photograph of the counter electrode loaded with NG.

To identify the doping of nitrogen atoms into graphene framework and the reduction of oxygen-containing species during hydrothermal reaction, the infrared spectra (IR) of GO and NG-12 were measured and displayed in Fig. 2. In the spectrum of GO, the peaks located at 3411 and 1051 cm^{-1} are attributed to the stretching vibration of hydroxyl groups. The peaks at 1732 and 1271 cm^{-1} are assigned to the stretching vibrations of C=O and C-O-C in conjugated graphene, respectively. After hydrothermal reaction, the height of the peak at 3411 cm^{-1} decreases accordingly. A weak peak at 1732 cm^{-1} is identified, which is assigned to the residual C=O groups surviving from the reduction process. More importantly, the peak at 1624 cm^{-1}, corresponding to the in-plane vibration of C=C, shifts to 1556 cm^{-1}. This is due

to the superposition of the vibrations of C=C and C=N, which gives the evidence of the embedding of nitrogen-containing groups. [38,53]

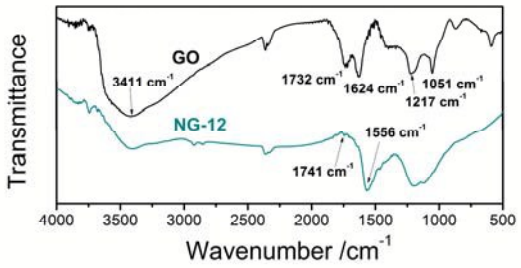

Fig. 2 FT-IR spectra of nitrogen doped graphene and graphene oxide.

Chemical composition of NG sheets was detected by using XPS. Fig. 3a displays the XPS spectra of the NG samples. It is indicated that nitrogen species are embedded into the graphene skeleton after hydrothermal reaction of 2 hrs. Compared with the XPS spectrum of GO, the curves of NG show that the doping of nitrogen atoms is accompanied by the reduction of oxygen groups. However, we further found that the oxygen groups in the graphitic framework cannot be reduced entirely even the time of hydrothermal preparation is prolonged to 18 hrs. In Fig. 3b, the XPS curves of the NG samples annealed at 350 °C are depicted. These curves illuminate the coexistance of nitrogen and oxygen groups in graphitic architecture after heat treatment. Thereby, the catalysis activities of the NG electrodes are probably originated from the contributions of both the nitrogen-containing groups and the residual oxygen species.

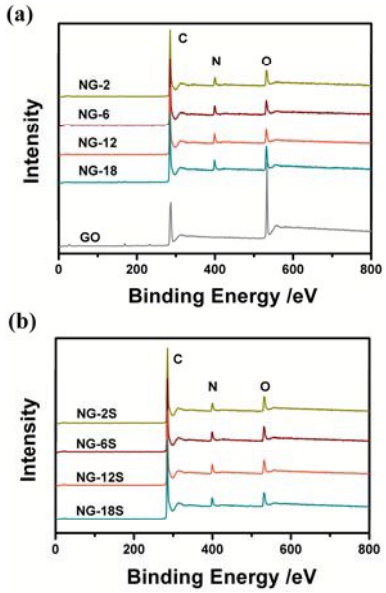

Fig. 3 X-ray photoelectron survey spectra of nitrogen doped graphene samples dried at 80°C (a) and annealed at 350 °C (b). XPS spectrum of graphene oxide is indicated in image (a) for comparison.

By evaluating XPS spectra, we summarized N and O contents of the NG sheets in Fig. 4. It is found that the nitrogen content of the NG-2 sample is as high as 7.3 at%. This demonstrates that urea is a promising nitrogen source for preparing NG via hydrothermal process. Further prolonging the reaction time to 12 hrs, nitrogen content merely increases 0.3 at%. When the hydrothermal preparation is performed for 18 hrs, however, nitrogen content drops to 6.7 at%. In Fig. 4, we show the atom content of the NG samples prepared with various time of hydrothermal reaction. Not surprisingly, oxygen content decreases successively with the hydrothermal reaction. However, an increase of oxygen content to 12.5 at% was observed at 18 hrs. We have confirmed that this anomalous result is reproductive. It is probably understood as the adsorption of monoxide on the surfaces or interlayers of NG nanosheets. The monoxide molecules in the closed autoclave are generated by the decarbonylation reactions of aromatic amide intermediates (forming pyrrolic groups) in graphene framework.[39,54] And the adsorption of monoxide on graphene has been well demonstrated and utilized for fabricating gas sensors with a ultra-high resolution.[55] Nevertheless, the total content of N and O atoms is less than that of GO (29.4 at%) by ~1/3, indicating the dual functions of urea in hydrothermal reaction, i.e. the embedding of N atom and the reduction of oxygen containing groups.

Elemental composition of the NG samples after annealing at 350°C is also depicted. Interestingly, heat treatment to NG-2 causes the decrease of nitrogen content from 7.3 to 5.5 at%. Similar phenomenon is also observed for the samples of NG-6. When the hydrothermal reaction exceeds 12 hrs, nitrogen content of the NG sheets after annealing becomes invariant. These results imply that the nitrogen groups embedded at the early stage of hydrothermal reaction are probably unstable to heating. With the proceeding of the reaction, the doped nitrogen groups turn to thermal-stable states. Additionally, a slight decrease of oxygen content by annealing is observed for the samples fabricated via hydrothermal reaction for 2~12 hrs. Notably, the annealing process results in the reduction of the oxygen content of NG-18 from 12.5 to 8.8 at%. It supports our hypothesis that the anomalous increase of oxygen content at the hydrothermal reaction time of 18 hrs arises from the adsorption of monoxide onto graphene sheets.

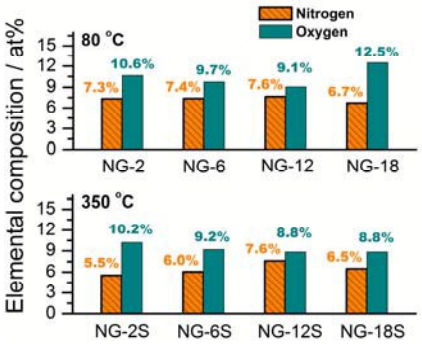

Fig. 4 XPS results of elemental composition of nitrogen doped graphene sheets annealed at 80 °C and 350 °C.

The high-resolution N1s, O1s, and C1s XPS spectra are further displayed for uncovering the doped nitrogen groups and unreduced oxygen species of the NG sheets. Fig. 5 shows the fitting examples for NG-12 and NG-12S. In Fig. 5a, the N1s spectrum is asymmetric, which could be decomposed into four peaks, corresponding to the bonding configurations of pyridinic

N (398.5 eV), pyrrolic N or aromatic amine N (399.8 eV), quaternary N (401.1 eV), and N-oxides of pyridinic N (402.8 eV), respectively. It is seen that hydrothermal reaction results in the primary bonding states of pyridinic N and pyrrolic N in NG framework. After annealing the NG sheets, parts of the two nitrogen groups converts into more thermal-stable quaternary N as illuminated in Fig. 5b. The XPS spectra of O atoms in the NG sheets after hydrothermal reaction and the successive heat treatment are indicated in Fig. 5c and d. The divided peaks at 530.9, 532.0, and 533.5 eV are designated to the oxygen atom with C-O bond, C=O bond, and O-C=O bond, respectively. It is apparent that heat treatment results in the variations of the relative content of oxygen containing groups. Moreover, the C1s spectra are shown in Fig. 5e and f. We observed the C=C peak is centered at 284.6 eV, corresponding to the sp^2 C atoms. A broad tail at higher binding energies indicates various states of the C atoms binding to N or O atoms. It was found that the C1s peaks can be well fitted by including the following binding states: C=N (285.3 eV), C – O & C−N (286.2 eV), C=O (287.8 eV), and O-C=O (289.2 eV).

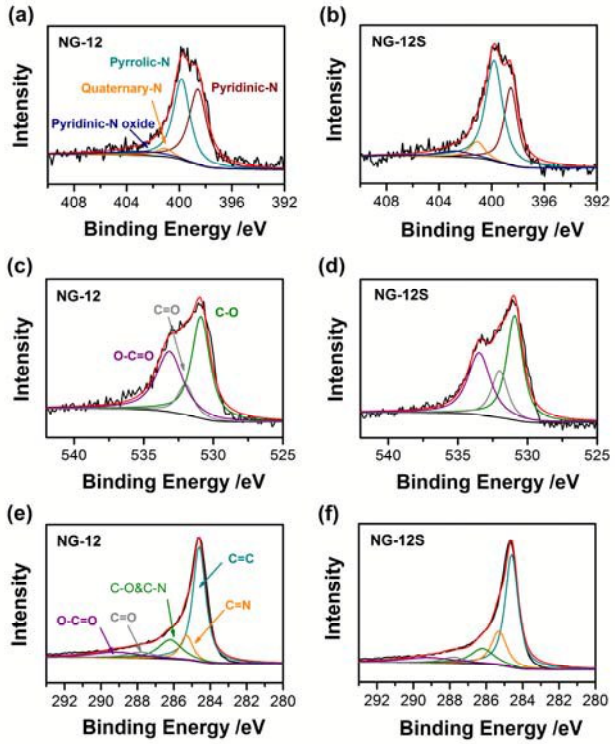

Fig. 5 High-resolution N1s (a and b), O1s (c and d), and C1s (e and f) spectra of nitrogen-doped graphene.

The contents of nitrogen and oxygen atom at various binding states are displayed in Fig. 6. The corresponding data are summarized in Table S1 and S2 (ESI†) in detail. Interestingly, the composition of nitrogen groups varies slightly when the time of hydrothermal reaction is in the range of 2 to 12 hrs. The primary bonding states of N atoms are pyridinic N and pyrrolic N. The atomic ratio of pyridinic N to pyrrolic N merely varies from 0.82 to 0.99. When the NG sheets are prepared hydrothermally for 18 hrs, the atomic content of pyridinic N descends evidently. At the same time, the content of quaternary N increases from 0.36 at% (NG-12) to 1.03 at%. It has been demonstrated that pyridinic N is thermally unstable relative to pyrrolic N.[48] Thereby, a part of the pyridinic groups are transformed to the state of quaternary N in the late stage of hydrothermal reaction. Fig. 6b indicates the effects of annealing on the composition of nitrogen atom at various binding states. We found that heat treatment to NG-2 results in the reduction of the atomic content of pyridinic N from 3.17 to 1.40 at%. Meanwhile, the content of pyridinic-N oxides increases from 0.49 to 1.18 at%. Similar result is also observed for the NG-6 samples. Furthermore, it is apparent that the amount of pyridinic-N groups surviving from annealing increases with the time of hydrothermal reaction. It implies that the hydrothermal reaction not only plays a role in embedding N atoms into graphene framework but also improve the thermal stability of pyridinic N groups. Therefore, more pyridinic-N groups are detected in the sample of NG-12S, which are crucial to improve electrocatalytic activity of NG sheets.

According to the variations of atomic content of pyridinic N and pyridinic-N oxides, a possible route to the removal of pyridinic groups during annealing could be suggested. Firstly the pyridinic groups formed in hydrothermal reaction are converted into pyridinic-N oxides. Afterwards, the pyridinic-N oxides are decomposed under the oxygen atmosphere. Moreover, the enhanced thermal stability of pyridinic groups upon hydrothermal reaction can be explained as following. The pyridinic groups, as many works demonstrated,[39,48] usually locate at the edge of graphene. Some of them maybe less conjugated to graphene framework, which are relatively easier to be removed or transformed into pyrrolic-N and quaternary N groups by heat treatment. However, hydrothermal reaction causes the reduction of oxygen groups and the self-healing of graphene framework. As a consequence, the pyridinic groups are probably embedded into the graphene structure, and hence become more conjugated and hence thermally stable.

Aside from the oxidation of pyridinic groups by annealing, the nitrogen loss is also probably caused by the removal of aromatic amine or amide groups. This is partly because the atomic contents of pyrrolic N, which includes the contribution of aromatic amine N, for the reaction time of 2, 6 hrs are reduced by annealing. When the reaction time exceeds 12 hrs, no apparent loss of nitrogen atoms is observed. It indicates a large part of aromatic amine or amide moieties is converted to more thermally stable pyrinidic or pyrrolic groups.Therefore, the hydrothermal reaction from 2 to 12 hrs is not useless for improving the electrocatalytic performance of NG sheets although the nitrogen content has no evident increase. Instead, the thermal-stability of N groups is improved evidently, which is of importance to the NG sheets serving as the cathode in DSC.

The variations of the composition of oxygen-containing groups are shown in Fig. 6c and d. We found that, during the process of hydrothermal reaction, the C=O bond are easy to be reduced to C-O bond or converted onto O-C=O bond via esterification. However, the anomalous increase of content of C=O bond for NG-18 sample, as we have addressed, is probably caused by the adsorption of the carbon monoxide molecules to the graphene sheets. This statement is based on the fact that the embedded C=O groups in the NG-18 sample are thermally unstable. After heat treatment, the content of C=O band becomes a normal value

of 0.64 at%.

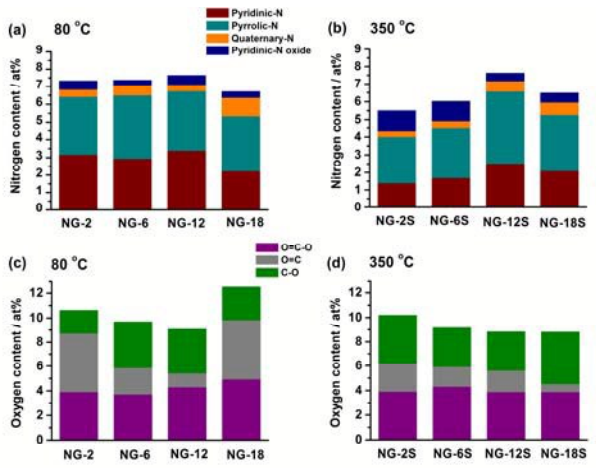

Fig. 6 Content distributions of N species (a and b) and O species (c and d).

The electrocatalytic activities of NG based electrodes were examined by using symmetrical dummy cells.[31] In these sandwich-type devices, two identical NG electrodes were separated with the distance of ~60 μm. The resultant space was filled by $Co(phen)_3$ based electrolyte for simulating the redox reactions of NG cathodes occurring in DSCs. Electrochemical impedance measurements at zero bias voltage were applied to the NG electrodes annealed at 80 and 350 °C. The corresponding impedance spectra are indicated in Fig. 7a and b, respectively. In this way, we aim to figure out the effects of annealing on electrocatalytic performance of NG electrodes on the basis of the impedance results. As demonstrated above, the NG cathodes fabricated in this work show porous rather than planar morphology. For this reason, diffusion impendance of cobalt redox couples shuttling in the porous NG layers cannot be ignored. Herein, we employed the equivalent circuit suggested by Roy-Mayhew et al. for fitting the impedance data of porous graphene electrodes.[33,34] As shown in the inset of Fig. 7a, the equivalent circuit is constituted by ohmic serial resistance (R_s), charge transfer resistance at NG sheet/electrolyte interfaces (R_{ct}), constant phase element (CPE), and Nernst diffusion impedance in the bulk electrolyte (Z_w) and the porous NG layer (Z_{pore}), respectively. The solid curves in Fig. 4a and b demonstrate that the used equivalent circuit enables a good fitting of the impedance data. Note that the fitting results will become unacceptable if the Z_{pore} element is excluded from the equivalent circuit.

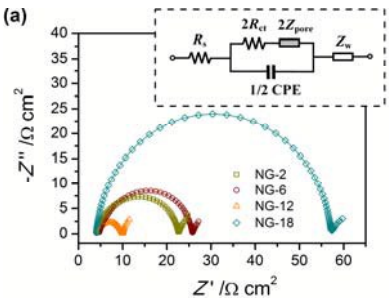

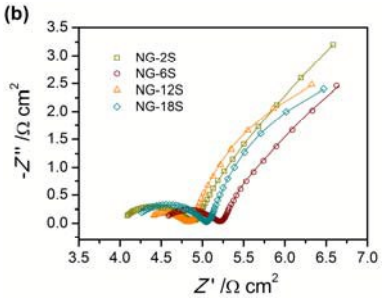

Fig. 7 Impedance spectra for symmetric dummy cells fabricated with nitrogen doped graphene electrodes dried at 80°C (a) and annealed at 350 °C (b). Inset of (a) shows the used equivalent circuit.

The fitting results according to the impedance data in this work are indicated in Fig. 8. The interfacial charge transfer resistances shown in Fig. 8a are plotted against the hydrothermal reaction time. We can see that the NG electrodes free from annealing exhibit R_{ct} ranging from 5.6 to 53 Ω cm^2 in dummy cells. And the minimal R_{ct} is achieved when the hydrothermal reaction in the preparation of NG sheets is terminated at 12 hrs. In comparison, the R_{ct} of the annealed NG electrodes is about 10~50 times lower that of the annealing-free samples. And a minimum R_{ct} of 0.58 Ω cm^2 is attained by the samples of NG-12S. The fitting data of R_{ct} allow us to estimate the exchange current density (J_0) by using the following expression,

$$J_0 = \frac{RT}{nFR_{ct}} \quad (1)$$

where R represents the gas constant, F is the Faraday constant, T is the absolute temperature and n stands for the number of the exchanged electrons (it equals to unity for the cobalt complexes). The plots of J_0 as a function of hydrothermal reaction time are depicted in Fig. 8b. These curves indicate unambiguously the crucial role of annealing in improving the electron transfer at electrolyte/NG interfaces. Aside from the effects of the heat treatment, the J_0 is highly relative to the elemental composition of NG sheets since the hydrothermal reaction time determines N and O contents directly. It is likely that the increase of nitrogen content and the concomitant decrease of oxygen content cause the improvement of J_0. The embedding of nitrogen atoms plays a role in enhancing the electrocatalytic activities of the NG sheets, while the reduction of oxygen groups facilitates the electron transport inside NG matrix. This explanation is also applicable to the catalytic behaviour of NG-18 samples. Lower value of J_0 is attributed to the higher oxygen content of 12.5 at% in combination with lower nitrogen content of 6.7 at%. In practice, several works have demonstrated that the enhanced electrocatalytic activity of GO electrode by reducing parts of oxygen-containing groups.[31,32] Although detailed mechanism is still debatable, it is certain that rapid electron conduction is ultimate to the NG sheets serving as redox active layer.

The impedance of the CPE element parallel to charge transfer resistance and Nernst diffusion impedance of porous NG sheet is given by

$$\mathrm{CPE} = B(i\omega)^{-\beta} \quad (2)$$

where B and β are frequency independent parameters. Roughly speaking, the annealing treatment results in the increase of the B value by one order of magnitude. Particularly when the hydrothermal reaction time is less than 12 hrs, the B value is reversely proportional to R_{ct}. This is in agreement with the EIS results of graphene nanoplatelet cathodes reported by Kavan et al.[56] In addition, the value of β for the NG samples without heat treatment is higher than 0.88. In contrast, the β value is below 0.78 when the NG electrodes were annealed. In the former case, diffusion of cobalt complexes in porous NG matrix is less important due to large value of R_{ct}. Accordingly, the redox reaction in the NG matrix can be regarded as the simple parallel circuit of charge transfer resistance and capacitance, which results in near-ideal value of β. In the latter case, however, the value of R_{ct} is comparable to that of Z_{pore}, which may cause the apparent deviation of β from unity. Additionally, we found that the annealing also affects the value of Z_{pore}. Figure 8d shows a lower value of Z_{pore} with the annealing process, implying the heat treatment alters the pores of NG sheets and facilitates the shuttling of cobalt complexes. This explanation is in agreement with the weight loss of the NG sheets (~0.51 mg cm^{-2}) by heat treatment. In view of the fitting results of Z_{pore} and R_{ct}, we found that effects of the diffusion of cobalt complexes on the electrocatalytic reaction cannot be ignored when the R_{ct} is decreased considerably by heat treatment.

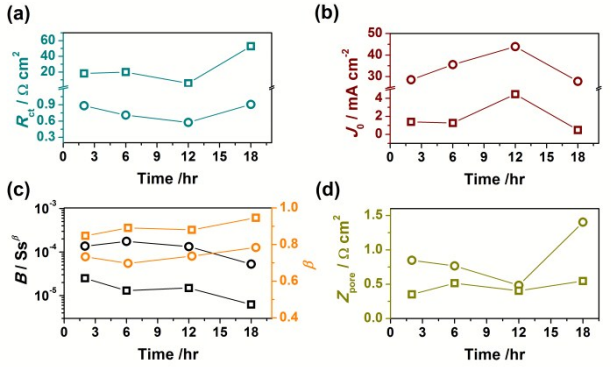

Fig. 8 Electrochemical Parameters for symmetric dummy cells fabricated with nitrogen doped graphene electrodes. Squares and Circles in the images mark the sample electrodes dried at 80°C and annealed at 350 °C, respectively.

To get a further insight on the reaction and diffusion of cobalt redox couples in the porous NG matrix, we plot R_{ct} and Z_{pore} against the bias voltage applied to the dummy cells during impendance measurements. As indicated in Fig. 9a, the decrease of R_{ct} with bias voltage is in agreement with the observations by Roy-Mayhew et al.[33] It is worthwhile to note that the charge transfer resistances of NG-6 over the whole range of bias voltage are higher than those of NG-6S, reflecting the effectiveness of heat treatment on improving the electrocatalytic activity of NG. Moreover, Z_{pore} is found to increase with bias voltage. It can be explained as the depletion of cobalt complexes in the porous NG layer.[56] It is evident that the Z_{pore} of NG-6S is more sensitive to bias voltage than that of NG-6. This is because the depletion is easier to occur at the surfaces of NG-6S for its much lower R_{ct}. Obviously, mass transport of cobalt based electrolyte in the NG layer has a profound influence on the electrocatalytic performance. It implies a future work on exploring the NG electrodes with the optimized morphology facilitating the shuttling of cobalt complexes.

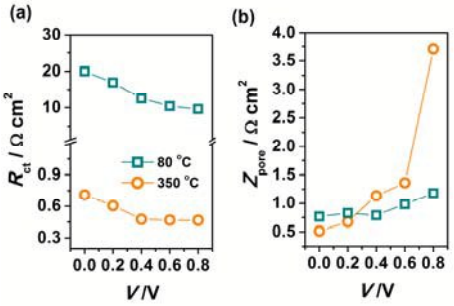

Fig. 9 Plots of charge transfer resistance (a) and Nernst diffusion impedance in porous NG layer (b) as a function as bias voltage. The NG sheets were prepared by hydrothermal reaction of 6 hrs.

Current density-voltage (J-V) characteristics of the DSCs with NG cathodes are shown in Fig. 10. The corresponding cell parameters are summarized in Table 1. It is seen that the DSCs based on NG-12 sample yield the power conversion efficiency (PCE) of 7.7 %, higher than those prepared hydrothermally in 2, 6, and 18 hrs. When the NG cathode was annealing at 350°C before cell assembly, the PCE of the DSCs is further improved to 8.2 %, exceeding the efficiency of the DSCs based on Pt cathode. Open circuit voltage (V_{oc}) and short circuit current density (J_{sc}) are 0.826 V and 16.6 mA cm^{-2}, respectively. The impedance spectra of the dummy cells containing NG-12S and platinized cathode are indicated in Fig. S3 (ESI†). Fitting result indicates that the R_{ct} of NG-12S cathode is 0.57 Ω cm^2, which is about 3 times lower than that of Pt cathode, affording its higher photocurrent. It is apparent that the hydrothermal reaction time is a determinent factor to the performance of NG cathodes during

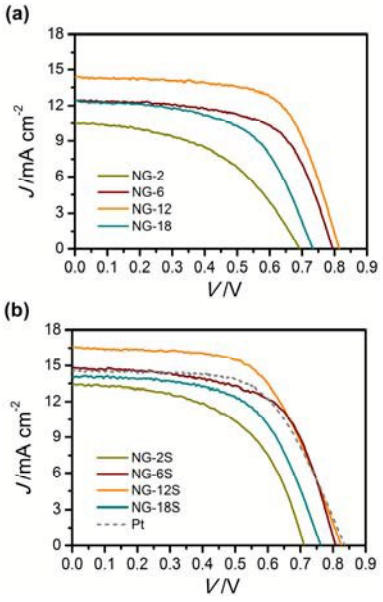

Fig. 10 J–V characteristics of the DSCs based on nitrogen doped graphene cathode after drying at 80°C (a) and annealing at 350 °C (b). All cells were irradiated under the simulated solar light of 100 mW cm^{-2}.The J–V curve of the DSCs with Pt cathode is shown in image (b) as a reference.

cell operating. More strictly, cell parameters are relative to the elemental composition of NG. Herein, the N/O ratio is also shown in Table 1 for illuminating these relations. For the NG electrodes with or without heat treatment, larger N/O ratio leads to higher values of PCE and J_{sc}. This reflects the dominant role of nitrogen-containing groups in improving the electrocatalytic activities of NG cathodes. In addition, the variation of J_{sc} with the hydrothermal reaction time is in agreement with the results of J_0 from impedance fitting. And it is notable that higher N/O ratio roughly results in a better value of fill factor (FF). It is known that fill factor is determined by various resistances of cell elements, such TiO_2 film, electrolyte solution, and cathode. In this work, only the chemical composition of the cathodes is varied. Therefore, the improvement of FF is probably attributed to the increase of N/O ratio since it decreases the overpotential of the electron transfer at electrolyte/NG interfaces.

Table 1 Photovoltaic parameters of the DSCs based on the NG electrodes with various N/O Ratios [a]

Cathode	N/O / at/at	V_{oc} /V	J_{sc} /mA cm^{-2}	FF	PCE /%
NG-2	0.689	0.694	10.5	0.48	3.5
NG-6	0.763	0.799	12.5	0.62	6.2
NG-12	0.835	0.818	14.4	0.66	7.7
NG-18	0.536	0.738	12.4	0.57	5.2
NG-2S	0.539	0.710	13.4	0.55	5.2
NG-6S	0.652	0.812	14.8	0.62	7.4
NG-12S	0.864	0.826	16.6	0.60	8.2
NG-18S	0.739	0.768	14.0	0.59	6.4
Pt		0.837	14.5	0.61	7.4

[a] All cells were irradiation under different intensities of simulated solar light (AM1.5). *V*oc: open circuit voltage, *J*sc: short circuit current density, FF: fill factor, PCE: power conversion efficiency. The active area of the DSCs is 0.156 cm^2.

In Fig.11, we show the impendance spectra of the DCS based upon the cathodes of NG-12, NG-12S, and Pt. By fitting the impendance data with the equivalent circuit in Fig. S5 (ESI†), charge transfer resistances (R_{ct}) for NG-12, NG-12S, and Pt are determined as 12.4, 0.632, and 1.15 Ω cm^2, respectively. It agrees qualitatively with the fitting results of the dummy cells, showing the key role of annealing in enhancing electrocatalytic activity. Also the Z_{pore} of NG-12S is 6.2 Ω cm^2, which is about twice higher than that of NG-12. It is because the depletion of redox couples is more apparent in the annealed NG layer as we have addressed.

4. Conclusions

Nitrogen doped graphene (NG) is a promising candidate when serving as a Pt-free cathode for cobalt complex based DSCs. However, the improvement of the NG based cathodes requires a deeper insight on the electrocatalytic activities of the embedding nitrogen groups as well as the unreduced oxygen species. In this study, we prepared nitrogen doped graphene via inhomogeneous hydrothermal process by using urea as a cheap nitrogen source. The electrocatalytic performance of the NG cathodes can be improved by increasing the N/O ratio. And a notable improvement of the catalytic activities is further realized by annealing the NG cathodes before assembling into DSCs. Upon this procedure, the cobalt based DSCs yield an optimized power conversion efficiency of 8.2 %. By fitting the XPS spectra, we found that the embedding nitrogen groups in the early stage of hydrothermal reaction are thermally unstable. By extending time of hydrothermal reaction, thermal stability of the nitrogen groups, including pyridinic-N, pyrrolic N, and quaternary N, is improved remarkably. This is quite helpful to maintain a higher N/O ratio from heat treatment and hence attain a state-of-art NG cathode.

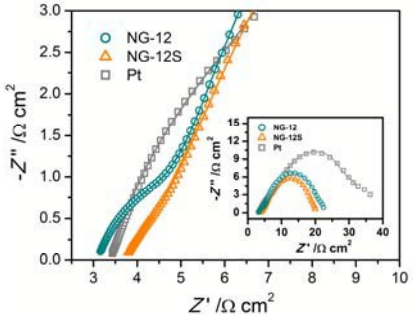

Fig.11 Impendance spectra at high frequency for the DSCs with NG electrodes annealed at 80 and 350 °C. The Impendance curve of the device based on Pt cathode is shown for comparison. Inset shows the impendance spectra over a full frequency range.

Acknowledgements

The support of the National Nature Science Foundation of China (21103123) and Tianjin Natural Science Foundation (13JCZDJC32400) is gratefully acknowledged.

Notes and references

Tianjin Key Laboratory of Organic Solar Cells and Photochemical Conversion, School of Chemistry & Chemical Engineering, Tianjin University of Technology, Tianjin 300384, P. R. China. E-mail: zhesun@tjut.edu.cn, xuesong@ustc.edu.cn; Fax: +86-22-60214252 Tel: +86-22-60214250

† Electronic Supplementary Information (ESI) available: chemical formulas of sensitizer XS57, photograph of NG/urea precusors, EIS of NG-12S and Pt cathodes, fitting results of atomic contents of nitrogen and oxygen at various states . See DOI: 10.1039/b000000x/

1 B. C. O'Regan and M. Grätzel, *Nature*, 1991, **353,** 737.
2 L. Peter, *J. Phys. Chem. Lett.*, 2011, **2**, 1861.
3 M. A. Green, K. Emery, Y. Hishikawa and W. Warta, *Prog. Photovoltaics* 2011, **19**, 84.
4 M. Liang and J. Chen, *Chem. Soc. Rev.*, 2013, **42**, 3453.
5 G. Boschloo and A. Hadfeldt, *Acc. Chem. Res.*, 2009, **42**, 1819.
6 J. G. Rowley, B. H. Farnum, S. Ardo and G. J. Meyer, *J. Phys. Chem. Lett.*, 2010, **1**, 3132.
7 M. Wang, C. Grätzel, S. M. Zakeeruddin and M. Grätzel, *Energy Environ. Sci.*, 2012, **5**, 9394.
8 H. Tian and L. Sun, *J. Mater. Chem.*, 2011, **21**, 10592.
9 T. Stergiopoulos and P. Falaras, *Adv. Energy Mater.*, 2012, **2**, 616.

10 S. Mathew, A. Yella, P. Gao, R. Humphry-Baker, B. F. E. Curchod, N. Ashari-Astani, I. Tavernelli, U. Rothlisberger, M. K. Nazeeruddin and M. Grätzel, *Nat. Chem.*, 2014, **6**, 242.

11 A. Yella, H. Lee, H. Tsao, C. Yi, A. Chandiran, M. Nazeeruddin, E. Diau, C. Yeh, S. Zakeeruddin and M. Grätzel, *Science* 2011, **334**, 629.

12 A. Yella, C. Mai, S. M. Zakeeruddin, S. Chang, C.-H. Hsieh, C. Yeh and M. Grätzel, *Angew. Chem. Int. Ed.*, 2014 , **53** , 2973.

13 J.-H. Yum, E. Baranoff, F. Kessler, T. Moehl, S. Ahmad, T. Bessho, A. Marchioro, E. Ghadiri, J.-E. Moser, C. Yi, M. K. Nazeeruddin and M. Grätzel, *Nat. Commun.*, 2012, **3**, 631.

14 Y. Bai, Q. Yu, N. Cai, Y. Wang, M. Zhang and P. Wang, *Chem. Commun.*, 2011, **47**, 4376.

15 J. Burschka, V. Brault, S. Ahmad, L. Breau, M. K. Nazeeruddin, B. Marsan, S. M. Zakeeruddin and M. Grätzel, *Energy Environ. Sci*., 2012, **5**, 6089.

16 D. Li, H. Li, Y. Luo, K. Li, Q. Meng, M. Armand and L. Chen, *Adv. Funct. Mater.*, 2010, **20**, 3358.

17 H. Tian, X. Jiang, Z. Yu, L. Kloo, A. Hagfeldt and L. Sun, *Angew. Chem. Int. Ed.*, 2010, **49**, 7328.

18 Y. Liu, J. R. Jennings, M. Parameswaran and Q. Wang, *Energy Environ. Sci.*, 2011, **4**, 564.

19 S. Das, P. Sudhagar, S. Nagarajan, E. Ito, S. Y. Lee, Y. S. Kang and W. Choi, *Carbon* 2012, **50**, 4815.

20 H. Bi, W. Zhao, S. Sun, H. Cui, T. Lin, F. Huang, X. Xie and M. Jiang, *Carbon* 2013, **61**, 116.

21 J.Y. Lin, C.Y. Chan and S.W. Chou, *Chem. Commun*., 2013, **49**, 1440.

22 B.-W. Park, M. Pazoki, K. Aitola, S. Jeong, E. M. J. Johansson, A. Hagfeldt and G. Boschloo, *ACS Appl. Mater. Interfaces*, 2014，**6**, 2074.

23 K. S. Novoselov, A. K. Geim, S. V. Morozov, D. Jiang, Y. Zhang, S. V. Dubonos, I. V. Grigorieva and A. A. Firsov, *Science*, 2004 , **306**, 666.

24 M. D. Stoller, S. Park, Y. Zhu, J. An and R.S. Ruoff, *Nano Lett.*, 2008 , **8**, 3498.

25 L. Kavan, J.-H. Yum, M. Graetzel, *Electrochim. Acta*, 2014, **128**, 349.

26 H. Wang, T. Maiyalagan and X. Wang, *ACS Catal.*, 2012, **2**, 781.

27 L. Song, Q. Luo, F. Zhao, Y. Li, H. Lin, L.T. Qu and Z.P. Zhang, *Phys. Chem. Chem. Phys.*, 2014, **16**, 21820.

28 D. Chen, H. Feng and Li, J. *Chem. Rev.*, 2012, **112**, 6027.

29 F. Pan, J. Jin, X. Fu, Q. Liu and J. Zhang, *ACS Appl. Mater. Interfaces*, 2013, **5**, 11108.

30 Z.G. Wang, P.J. Li, Y.F. Chen, J.R. He, W.L. Zhang, O.G. Schmidt, Y.R. Li, *Nanoscale*, 2014, **6**, 7281.

31 L. Kavan, J.-H. Yum, M. Graetzel, *ACS Appl. Mater. Interfaces*, 2012, **4**, 6999.

32 H.-S. Jang, J.-M. Yun, D.-Y. Kim, D.-W. Park, S.-I. Na, S.-S. Kim, *Electrochim. Acta*, 2012, **81**, 301.

33 J. D. Roy-Mayhew, D. J. Bozym, C. Punckt and I. A. Aksay, *ACSNano*, 2010, **4**, 6203.

34 J. D. Roy-Mayhew, G. Boschloo, A. Hagfeldt and I. A. Aksay. *ACS Appl. Mater. Interfaces*, 2012, **4**, 2794.

35 H. Wang, M. Xie, L. Thia, A. Fisher and X. Wang, *J. Phys. Chem. Lett.*, 2014, **5**, 119.

36 X. Li, H. Wang, J. T. Robinson, H. Sanchez, G. Diankov and H. Dai, *J. Am. Chem. Soc.*, 2009, **131**, 15939.

37 S. Hou, X. Cai, H. Wu, X. Yu, M. Peng, K. Yan and D. Zou, *Energy Environ. Sci.*, 2013, **6**, 3356.

38 M. J. Ju, J. C. Kim, H.-J. Choi, I. T. Choi, S. G. Kim, K. Lim, J. Ko, J.-J. Lee, I.-Y. Jeon, J.-B. Baek and H. K. Kim, *ACSNano*, 2013, **7**, 5243.

39 L. Sun, L. Wang, C. Tian, T. Tan, Y. Xie, K. Shi, M. Li and H. Fu, *RSC Advances*, 2012, **2**, 4498.

40 M.-Y. Yen, C.-K. Hsieh, C.-C. Teng, M.-C. Hsiao, P.-I Liu, C.-C. M. Ma,M.-C. Tsai, C.-H. Tsai, Y.-R. Lin and T.-Y. Chou, *RSC Adv.,* 2012, **2**, 2725.

41 D. Yu, L. Wei, W. Jiang, H. Wang, B. Sun, Q. Zhang, K. Goh, R. Si and Y. Chen, *Nanoscale*, **2013**, 5, 3457.

42 N. Papageorgiou , M. Grätzel and P.P. Infelta, *Sol. Energy Mater. Sol. Cells*, 1996, **44**, 405.

43 N. Papageorgiou, P. Liska, A. Kay and M. Grätzel, *J. Electrochem. Soc.*, 1999, **146**, 898

44 Z. Lei, L. Lu and X. S. Zhao, *Energy Environ. Sci.*, 2012, **5**, 6391.

45 D. C. Marcano, D. V. Kosynkin, J. M. Berlin, A. Sinitskii, Z. Sun, A. Slesarev, L. B. Alemany, W. Lu and J. M. Tour, *ACSNano*, 2010, **4**, 4806.

46 S. Ito, T. N.Murakami, P. Comte, P. Liska, C. Grätzel, M. K. Nazeeruddin, M. Grätzel, *Thin Solid Films*, 2008, **516**, 4613.

47 Z. Wang, M. Liang, L. Wang, Y. Hao, C. Wang, Z. Sun and S. Xue, *Chem. Commun.*, 2013, **49**, 5748.

48 L. Lai, J. R. Potts, D. Zhan, L. Wang, C. K. Poh, C. Tang, H. Gong, Z. Shen, J. Lin and R. S. Ruoff, *Energy Environ. Sci.*, 2012, **5**, 7936.

49 D. W. Boukhvalov and M. I. Katsnelson, *J. Phys. Chem. C*, 2009, **113**, 14176.

50 A. Buchsteiner, A. Lerf and J. Pieper, *J. Phys. Chem. B*, 2006, **110**, 22328.

51 Z.-H. Sheng, L. Shao, J.-J. Chen, W.-J. Bao, F.-B.Wang and X.-H. Xia, *ACSNano*, 2011, **5**, 4350.

52 D. Long, W. Li,; L. Ling, J. Miyawaki, I. Mochida and S.-H. Yoon, *Langmuir*, 2010, **26**, 16096.

53 Y. Xue, J. Liu, H. Chen, R. Wang, D. Li, J. Qu and L. Dai, *Angew. Chem. Int. Ed.*, 2012, **51**, 12124.

54 S. Stankovich, D. A. Dikin, R. D. Piner, K. A. Kohlhaas, A. Kleinhammes, Y. Jia, Y. Wu, S. T. Nguyen and R. S. Ruoff, *Carbon*, 2007, **45**, 1558.

55 F. Schedin, A. K. Geim, S. V. Morozov, E. W. Hill, P. Blake, M. I. Katsnelson and K. S. Novoselov, *Nat. Mater.*, 2007, **6**, 652.

56 L. Kavan, J.-H. Yum, M. K. Nazeeruddin and M. Grätzel, *ACSNano* 2011, **5**, 9171.